

## The Effect of Ni/AC and Mo/AC Catalyst Arrangements on the Activity and Selectivity for Hydrotreating Palm Cooking Oil into Biojet Fuel

Wega Trisunaryanti\*, Karna Wijaya, and Muhammad Darul Ikhsan Saputro

Department of Chemistry, Faculty of Mathematics and Natural Sciences, Universitas Gadjah Mada, Sekip Utara, Yogyakarta 55281, Indonesia

\* **Corresponding author:**

tel: +62-811256055

email: wegats@ugm.ac.id

Received: August 10, 2024

Accepted: February 20, 2025

DOI: 10.22146/ijc.99071

**Abstract:** This research was done to study the effect of the arrangement of nickel (Ni) and molybdenum (Mo) metals impregnated with activated carbon on the activity and selectivity of the hydrodeoxygenation (HDO) of palm cooking oil into biojet fuel. The catalysts were synthesized by impregnating Ni and Mo metals by dry spray impregnation method with precursor salts nickel(II) nitrate hexahydrate ( $\text{Ni}(\text{NO}_3)_2 \cdot 6\text{H}_2\text{O}$ ) and ammonium heptamolybdate tetrahydrate ( $(\text{NH}_4)_6\text{Mo}_7\text{O}_{24} \cdot 4\text{H}_2\text{O}$ ) solutions, respectively on the activated carbon. The catalysts were characterized using FTIR, XRD, SAA, SEM-EDX, and  $\text{NH}_3$ -TPD instruments. The catalyst performance was tested using a semi-batch reactor with dual heaters in a one-pot system, atmospheric pressure, and a hydrogen gas flow rate of  $20 \text{ mL min}^{-1}$  for the palm cooking oil HDO reaction for 3 h. The obtained liquid products were analyzed using gas chromatography-mass spectrometry (GC-MS). The best catalyst arrangement was the Ni/AC catalyst in a double-layer arrangement, which had 6.25 wt.% metal content, and a surface area of  $803.89 \text{ m}^2 \text{ g}^{-1}$  which resulted in 24.75 wt.% yield with 86.93% (fraction 1) and 87.48% (fraction 2) selectivity. This research concluded that catalyst layer arrangement affects the catalytic activity and selectivity in the HDO of palm cooking oil.

**Keywords:** activated carbon; biojet fuel; hydrodeoxygenation; nickel; molybdenum

### ■ INTRODUCTION

Every year, the global consumption of fossil fuels continues to rise, with the aviation sector being a major contributor. This sector's high demand has led to a significant increase in global carbon dioxide ( $\text{CO}_2$ ) emissions, accounting for 2.6% of the total, and contributing 5.9% to anthropogenic global greenhouse gas emissions in 2019 [1-2]. Fuel consumption is projected to increase from 4 quadrillion Btu in 2010 to 16 quadrillion Btu by 2050 [3]. The use of fossil fuels results in emissions of greenhouse gases such as methane ( $\text{CH}_4$ ), nitrous oxide ( $\text{N}_2\text{O}$ ), and  $\text{CO}_2$ , contributing to global warming [4-5]. Additionally, sulfur dioxide in the atmosphere can react with water vapor to produce acid rain [6]. Therefore, alternative environmentally friendly fuels are needed to reduce environmental pollution and address the declining availability of fossil fuels in the aviation sector. Biojet fuel is an environmentally friendly

alternative to address the declining availability of fossil fuels [7-8] with lower operating costs, energy consumption, and harmful production emission [9]. Biojet fuel production can be derived from palm oil. Processing palm oil is cheap and simple. Palm oil has been abundant and the most popular cooking oil worldwide since 2005, taking the place of soybean oil. In 2012, 52.1 million metric tons of palm oil were used worldwide, and Indonesia was one of the largest consumers [10]. Besides being used as food, palm oil can also serve as an alternative fuel. Currently, Indonesia is developing this alternative fuel to enhance energy security and reduce the country's vulnerability to fluctuations in global oil prices [11].

Palm oil is processed into various products, one of which is cooking oil. Cooking oil contains saturated and unsaturated fatty acids dominated by palmitic acid (C16:0) and oleic acid (C18:1). These compounds play a

crucial role in the hydrodeoxygenation (HDO) and hydrocracking processes of palm cooking oil into biojet fuel, with carbon chains ranging from C7 to C16 and hydrocarbon content such as *n*-alkanes, iso-alkanes, cycloalkanes, and aromatics [3,12]. HDO is a process to remove oxygen atoms without breaking the main chain as shown in Fig. 1 [13-14]. The HDO reaction was then followed by the hydrocracking process to obtain biojet fuel fractions. This process uses high temperature and pressure hydrogen gas to obtain the desired product

fractions, as shown in Fig. 2 [15-16]. A catalyst is essential to achieve optimal results in HDO reaction and hydrocracking.

Commercially developed HDO catalysts, such as Al<sub>2</sub>O<sub>3</sub> and SiO<sub>2</sub>, were designed for crude oil. However, palm oil contains carboxylic acids and C–O bonds, which these catalysts are not suited to break, necessitating the development of alternative catalysts [17]. For commercial HDO reactions on palm oil, palladium (Pd) and platinum (Pt) were used due to their

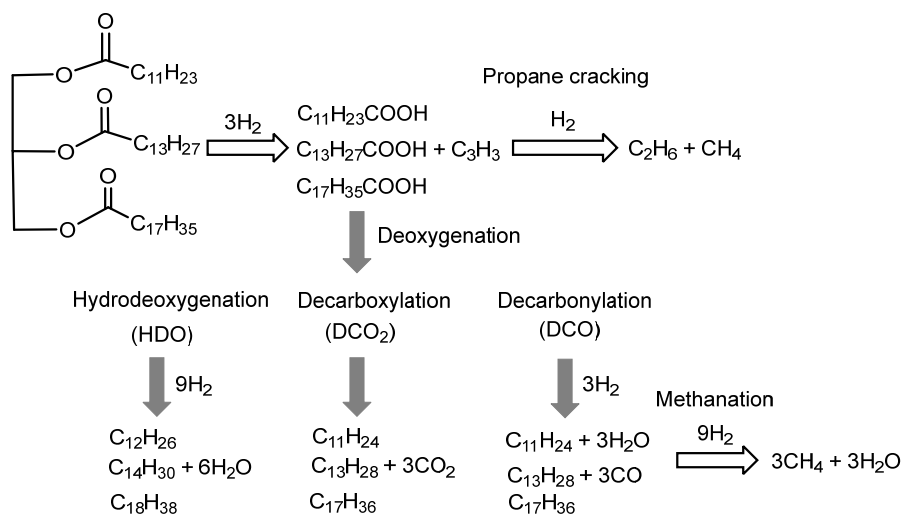


Fig 1. Hydrodeoxygenation reaction scheme

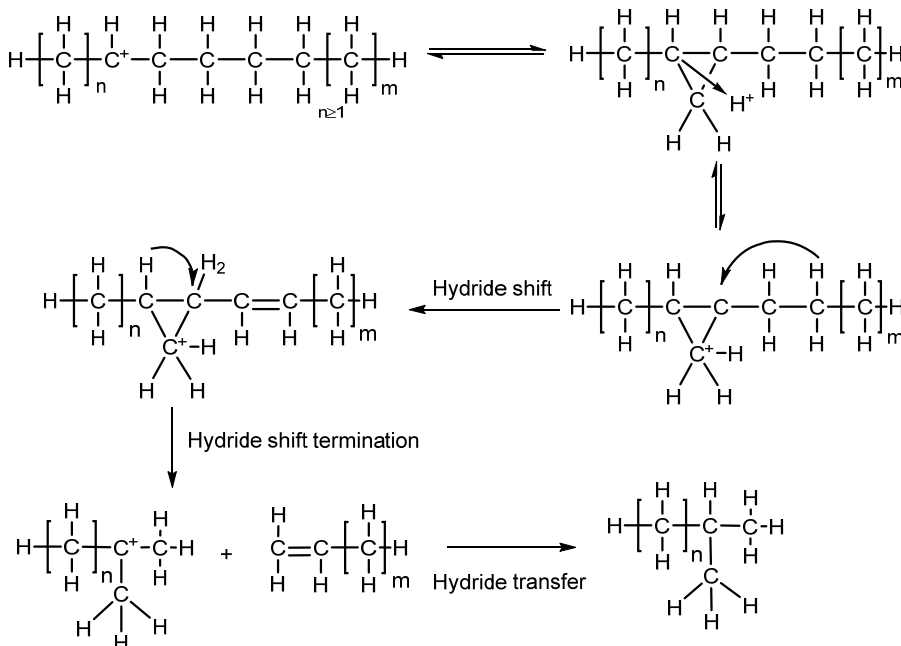


Fig 2. Palm cooking oil hydrocracking reaction mechanism

performance, resulting in high-quality biofuels. However, the increase in Pd and Pt metal scarcity resulted in high cost. Transition metals like nickel (Ni) and molybdenum (Mo) are more affordable than Pd and Pt, and they also have half-filled *d* orbitals [18-20]. These half-filled orbitals can accept electron pairs, thereby increasing the catalytic activity of the catalyst by breaking down the fatty acid of the palm oil into *n*-alkanes, iso-alkanes, cycloalkanes, and aromatics [21]. Vacant *p* orbitals and unpaired electrons in the *d* orbitals of nickel metals are able to accept electron pairs from the palm oil for HDO reaction [22-23]. Mo has 5 half-filled *d* orbitals that are reactive with the fatty acids of palm oil, leading to the breakage of CO bond of the fatty acids [24]. It is necessary to impregnate the metals into a support to ensure their uniform distribution and enhance the thermal stability of the catalyst [25]. Metal impregnation improves the catalyst's acidity sites and catalytic activity [26].

In order for the metal and palm oil feed to come into contact during the HDO reaction, there needs to be a support. This will increase the support's surface area, catalytic activity, and lifespan, and it will also stop the metals from sticking together, which lowers the catalytic activity, by making them stick to the support's surface. Activated carbon (AC) is a porous material with high porosity and surface area. AC has advantages in gas and liquid adsorption processes, making it suitable as a catalyst support [27-28]. This material can be synthesized from natural materials such as bituminous coal, peat, lignite, wood sawdust, and coconut shells. Additionally, AC can be produced from agricultural residues such as corn, corn cobs, bagasse, fruits, fruit pulp, and coffee beans. These raw materials are abundant, cheap, and readily available [29].

Metal impregnation onto the support was needed to increase the catalyst activity and selectivity during the HDO reaction. Dry impregnation with spraying method is used to uniformly disperse metals on the support by dissolving the metal in its precursor salt with a minimum amount of solvent. This method is highly effective in solvent utilization and achieving more uniform metal distribution compared to wet impregnation, which uses more solvent than dry impregnation, resulting in the risk

of losing the metal particles in the solvent and being more expensive on the cost [19,30-31].

In this study, variations in catalyst arrangements were conducted to study the effect on catalytic activity and selectivity. The catalyst arrangement has the potential for more selective catalysis, and each arrangement has a different role, potentially increasing catalytic activity. A study by Park et al. [32] showed that catalyst arrangement or stacking in the variation of noble and non-noble metal for anion-exchange membrane water electrolysis. However, such a method has not been applied to biofuel conversion. Therefore, current research has the novelty of utilizing single-layer and double-layer catalyst arrangements that were varied with the same weight of respective catalyst for biojet fuel conversion. These variations include Ni/AC single and double layers, Mo/AC single and double layers, as well as Ni/AC bottom layer and Mo/AC top layer.

## ■ EXPERIMENTAL SECTION

### Materials

The materials utilized in this study included Hemart Palm Oil from PT Bina Karya Prima, jet fuel samples from PT Pertamina, AC from Merck (102186), nickel(II) nitrate hexahydrate ( $\text{Ni}(\text{NO}_3)_2 \cdot 6\text{H}_2\text{O}$ ), ammonium heptamolybdate tetrahydrate ( $(\text{NH}_4)_6\text{Mo}_7\text{O}_{24} \cdot 4\text{H}_2\text{O}$ ) from Sigma-Aldrich. Deionized water was provided by CV Bima Aksara Nusa. Hydrogen ( $\text{H}_2$ ) and nitrogen ( $\text{N}_2$ ) gas were supplied by PT. Samator Gas Industri.

### Instrumentation

The analytical instrument that used were Fourier transform infra-red spectrometer (FTIR, Shimadzu IR Prestige-21), X-ray diffraction (XRD, Shimadzu XRD-6000), surface area analyzer (SAA, Quantachrome TouchWin v1.22), scanning electron microscope-energy dispersive X-ray (SEM-EDX, JEOL JED-2300), temperature-programmed desorption of ammonia ( $\text{NH}_3$ -TPD Micromeritics Chemisorb 2750), and gas chromatography-mass spectrometer (GC-MS, Shimadzu QP2010S with Rtx 5 MS and DB-5MS column).

## Procedure

### Synthesis of Ni/AC and Mo/AC catalysts

The impregnation of Ni and Mo metals, each with a content of 6 wt.%, into Activated Carbon was carried out using dry impregnation through spraying. The precursors used were  $\text{Ni}(\text{NO}_3)_2 \cdot 6\text{H}_2\text{O}$  and  $(\text{NH}_4)_6\text{Mo}_7\text{O}_{24} \cdot 4\text{H}_2\text{O}$ , respectively. The spray impregnation method was performed by spraying 42 mL of precursor solution into a spray bottle containing 14 g of AC in a porcelain dish until a paste formed. The catalysts impregnated with Ni and Mo metals were dried in an oven at 110 °C for 3–4 h. The catalysts were then calcined using  $\text{N}_2$  gas at a flow rate of 20 mL/min for 3 h at 500 °C and reduced using  $\text{H}_2$  gas at a flow rate of 20 mL/min for 3 h at 500 °C. The catalysts were analyzed using FTIR, XRD, SEM-EDX mapping, SAA, and  $\text{NH}_3$ -TPD. Calculations were conducted to determine the weight of Ni and Mo metals required for each metal with a concentration of 6%, as shown in Eq. (1) and (2). The synthesized catalysts using Ni and Mo metals impregnated onto activated carbon were labeled Ni/AC and Mo/AC, respectively.

$$\begin{aligned} & \text{Ni}(\text{NO}_3)_2 \cdot 6\text{H}_2\text{O} \text{ precursor weight} \\ &= \frac{\text{MrNi}(\text{NO}_3)_2 \cdot 6\text{H}_2\text{O}}{\text{ArNi}} \times C \times W_{\text{ka}} \end{aligned} \quad (1)$$

$$\begin{aligned} & (\text{NH}_4)_6\text{Mo}_7\text{O}_{24} \cdot 4\text{H}_2\text{O} \text{ precursor weight} \\ &= \frac{\text{Mr}(\text{NH}_4)_6\text{Mo}_7\text{O}_{24} \cdot 4\text{H}_2\text{O}}{7 \times \text{ArMo}} \times C \times W_{\text{ka}} \end{aligned} \quad (2)$$

The catalyst activity test was conducted with AC, Ni/AC, and Mo/AC catalysts in the hydrocracking and HDO reactions of palm oil feedstock into biojet fuel. This process was carried out with a catalyst-to-feed ratio of 1:100 (w/v) with an upper reactor temperature of 200 °C and a lower reactor that was divided into two fractions based on temperature ranges between 400–475 °C as fraction 1 (bottom) and 475–550 °C as fraction 2 (top).

Variations were performed on the single-layer and double-layer catalyst arrangements in the hydrocracking of palm oil using a semi-batch stainless-steel double-reactor system with a  $\text{H}_2$  gas flow rate of 20 mL/min. The catalyst arrangement variations consisted of Ni/AC single layer and Ni/AC double layers, Mo/AC single layer and Mo/AC double layers, and Ni/AC with Mo/AC layers with the same weight of 0.4 g of catalyst by stacking the

catalyst with separate catalyst containers. Calculations for liquid products conversion were calculated based on Eq. (3);

$$\text{Liquid products (wt. \%)} = \frac{W_{\text{product}}}{W_{\text{feed}}} \times 100\% \quad (3)$$

where  $W_{\text{product}}$  = liquid product weight (g) and  $W_{\text{feed}}$  = feed weight (g).

As for the biojet fuel, non-biojet fuel, oxygenated compounds, and main biojet fuel yield were calculated with the Eq. (4–7);

$$\text{Biojet fuel yield (wt. \%)} = \frac{A_{\text{b}}}{A_{\text{total}}} \times \frac{W_{\text{product}}}{W_{\text{feed}}} \times 100\% \quad (4)$$

$$\text{Non-biojet fuel yield (wt. \%)} = \frac{A_{\text{n}}}{A_{\text{total}}} \times \frac{W_{\text{product}}}{W_{\text{feed}}} \times 100\% \quad (5)$$

$$\text{Oxygenated yield (wt. \%)} = \frac{A_{\text{o}}}{A_{\text{total}}} \times \frac{W_{\text{product}}}{W_{\text{feed}}} \times 100\% \quad (6)$$

$$\text{Main biojet fuel yield (wt. \%)} = \frac{A_{\text{bp}}}{A_{\text{total}}} \times \frac{W_{\text{product}}}{W_{\text{feed}}} \times 100\% \quad (7)$$

The biojet fuel selectivity was calculated based on the Eq. (8);

$$\text{Selectivity} = \frac{A_{\text{b}} + A_{\text{bp}}}{A_{\text{total}}} \times 100\% \quad (8)$$

where  $A_{\text{b}}$  = GC spectra area of the biojet fuel fraction (%),  $A_{\text{n}}$  = GC spectra area of the non-biojet fuel fraction (%),  $A_{\text{o}}$  = GC spectra area of the oxygenated compound (%),  $A_{\text{bp}}$  = GC spectra area of the main biojet fuel fraction (%),  $A_{\text{total}}$  = Total GC spectra area percentage (%),  $W_{\text{product}}$  = Liquid product weight (g), and  $W_{\text{feed}}$  = Feed weight (g).

### HDO and hydrocracking of palm oil

Thermal testing was conducted with 40 mL of palm oil feedstock without catalyst. The process was carried out in a semi-batch stainless steel reactor system with dual heaters and a  $\text{N}_2$  gas flow rate of 20 mL/min as shown in Fig. 3. The upper reactor temperature was set with temperature variations of 175, 200, and 225 °C. The lower reactor temperature was incrementally raised in 25 °C increments every 5 min until reaching a temperature of 550 °C. The thermal temperature of palm cooking oil was determined as the temperature at which the first drop of vaporized oil condensed back into liquid during the thermal testing. The liquid products were

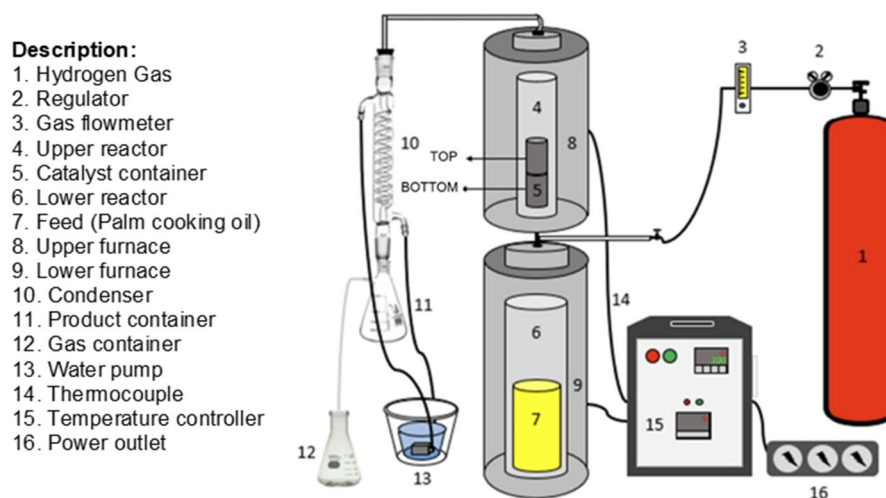


Fig 3. Semi-batch stainless steel reactor system with dual heaters schematic

collected with separation into two fractions based on temperature ranges between 400–475 °C as fraction 1 (bottom) and between 475–550 °C as fraction 2 (top). The obtained liquid product was analyzed by GC-MS using DB-5MS column with 40.0 and 250.0 °C of column and injection temperature, respectively. The temperature variations that had the highest product selectivity were used in the catalyst activity test.

## ■ RESULTS AND DISCUSSION

### Palm Oil Characterization

The composition of fatty acids in cooking oil using GC-MS is shown in Table 1. Palm cooking oil contains fatty acids, as analyzed by GC-MS using the Rtx 5 MS column, which was esterified first; thus, there is no triglyceride. The fatty acids that are presented in palm cooking oil range from carbon chain C15–C19, which falls within the biojet fuel hydrocarbon range. The predominant compounds found in cooking oil are oleic acid (43.73%) and palmitic acid (39.90%). Based on the

composition of these fatty acids, the application of catalysts through the hydrocracking and HDO processes of cooking oil has the potential to produce biojet fuel within the C7–C16 carbon chain range selectively.

### Catalyst Functional Group Characterization Using FTIR Spectrometer

The characterization of the functional group of AC, Ni/AC, and Mo/AC catalysts are displayed in IR spectra with wavelengths from 400 to 4000  $\text{cm}^{-1}$  using FTIR is shown in Fig. 4. The FTIR spectra contained in the catalyst material can be analyzed using an FTIR instrument to prove the success of metal impregnation on AC support by detecting the metal oxide functional groups. The bonding characteristics of a compound are determined based on the absorption of chemical bond vibrations. Based on Fig. 4, at the wavelengths 3413.17, 3435.66, and 3413.17  $\text{cm}^{-1}$ , a peak spectrum expansion indicates the presence of a hydroxy (OH) functional group [33]. In the catalysts Ni/AC and Mo/AC, there is

Table 1. Palm cooking oil composition analysis by using GC-MS

Retention time (min)	Similarity index	Compound name	Compound formula	Area (%)
25.087	95	Methyl myristate	$\text{C}_{15}\text{H}_{30}\text{O}_2$	0.70
29.244	97	Methyl palmitate	$\text{C}_{17}\text{H}_{34}\text{O}_2$	39.90
32.407	95	9,12-Hexadecadienoic acid	$\text{C}_{17}\text{H}_{30}\text{O}_2$	11.47
32.553	96	Methyl oleate	$\text{C}_{19}\text{H}_{36}\text{O}_2$	43.73
32.649	94	Methyl oleate	$\text{C}_{19}\text{H}_{36}\text{O}_2$	0.65
33.030	97	Methyl stearate	$\text{C}_{19}\text{H}_{38}\text{O}_2$	3.55

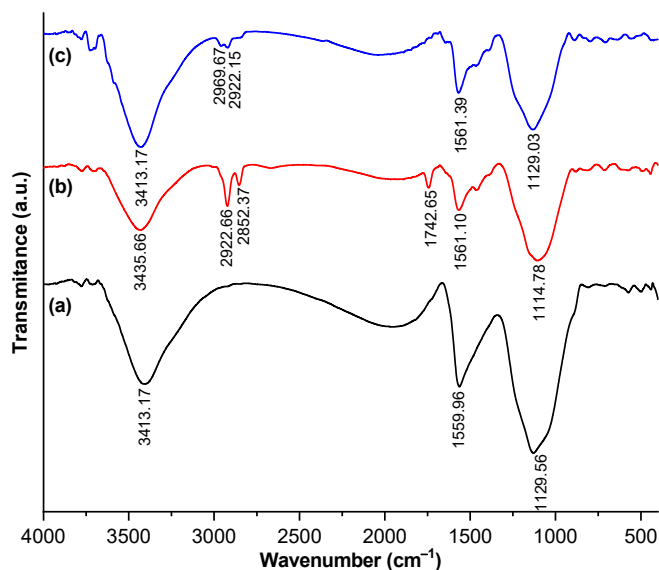


Fig 4. FTIR spectra of (a) AC, (b) Ni/AC, and (c) Mo/AC

Table 2. FTIR spectra interpretation of AC, Ni/AC, and Mo/AC catalysts

Wavenumber (cm <sup>-1</sup> )			Vibration type
AC	Ni/AC	Mo/AC	
1129.56	1114.78	1129.03	Stretching C–O
1559.96	1561.10	1561.39	Stretching C=C
-	1742.65	-	C=O
-	2852.37	2922.15	Stretching C–H
-	2922.66	2969.67	Stretching C–H
3413.17	3435.66	3413.17	Bending O–H

a decrease in OH group intensity caused by the calcination process at 500 °C. In the Ni/AC and Mo/AC catalyst, spectra appear at wavelengths 2852.37, 2922.66, 292.15, and 2969.67 cm<sup>-1</sup>, indicating symmetrical and asymmetric C–H stretching vibrations. Absorption at 1559.96, 1561.10, and 1561.39 cm<sup>-1</sup> indicates a C=C stretching vibration [34]. The wavenumber at 1742.65 cm<sup>-1</sup> shows the C=O functional group [35]. No C–C functional group exists because FTIR is more sensitive and accurate for detecting polar functional groups due to significant changes in dipole moments during molecular vibrations. The metal impregnation caused the C=O, OH, and C–H functional groups to show up. This, in turn, caused the AC to hydrogenate. The hydrogen came from the catalyst synthesis during the reduction process. Based on Fig. 2, the impregnation of Ni and Mo metals does not significantly affect the presence

of the functional groups. The results of catalyst FTIR spectrum interpretation is presented in Table 2.

### Catalyst Mineral Characterization Using XRD

Diffractiongram of AC, Ni/AC, and Mo/AC catalysts using XRD are shown in Fig. 5. The analysis using the XRD instrument aims to determine the mineral content of the catalysts. In addition, it also studied the effect of the impregnation of Ni and Mo metals on AC crystallinity. The mineral content was analyzed by comparing the diffraction angle data with the International Center for Diffraction Data (ICDD) and JCPDS databases using X'Pert Highscore software. The peak indicated by the diagram of Fig. 5 had some correspondence with the ICDD database for carbon/graphite material with ICDD number 00-008-0415 [36]. The peaks at 2θ of 23.95°, 62.49°, and 79.26° (marked as AC in Fig. 5(a)) indicate the characteristic diffraction of activated carbon. Peak of metal diphraz Ni appears at angles 2θ of 44.49°, 51.9°, and 76.4° (JCPDS 04-0850, ICDD 00-003-1051) as shown in Fig. 5(b) [37]. Meanwhile, the diffraction patterns of Mo metal show the presence of MoO<sub>2</sub> (ICSD 00-0320671) [38] and MoO<sub>3</sub> (ICCD 00-047-1081 and 005-0508) [39]. As seen in Fig. 5(c), MoO<sub>2</sub> peaks are observed at 2θ values of 36.98°, 43.50°, and 53.35° (YCP 04-085050), while MoO<sub>3</sub> peaks appear at 2θ values of 23.015°, 25.840°, and 27.335°.

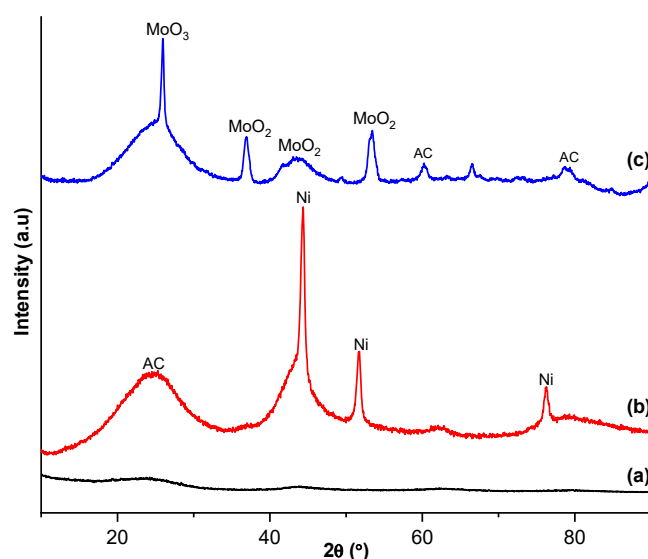


Fig 5. Diffractiongram of (a) AC, (b) Ni/AC, and (c) Mo/AC catalysts

These results indicate that the Mo/AC catalysts contain molybdenum in the form of MoO<sub>2</sub> and MoO<sub>3</sub> oxides.

As shown in Fig. 5, there is a diffractogram pattern that the AC catalyst has a peak width, indicating the material is amorphous. The Ni/AC and Mo/AC catalysts show a sharp peak of the crystal, indicating that the Ni and Mo metals have been successfully impregnated and can be seen from the degree of crystallinity. The crystallinity degrees of AC, Ni/AC, and Mo/AC catalysts are 25.5, 35.2 and 48.5%, respectively. Using Origin Pro software, the crystallinity degrees of activated carbon, Ni/AC, and Mo/AC catalysts are calculated by using the Eq. (9);

$$\text{Crystallinity} = \frac{A_{\text{peak}}}{A_{\text{total}}} \quad (9)$$

the  $A_{\text{peak}}$  is the XRD peak area (%), and  $A_{\text{total}}$  is the total XRD area (%). The crystallinity values indicate that the impregnation of Ni and Mo metals on the AC material causes amorphous changes in the structure into crystalline.

### Catalyst Surface Morphology Characterization Using SEM-EDX

Surface morphology, element content, and mapping of AC, Ni/AC, and Mo/AC catalysts using SEM-EDX are

shown in Fig. 6 and Table 3. AC has a fine morphology with a solid, long sheet structure based on Fig. 6(a). The metal impregnation on the AC, as seen by the blue circles in Fig. 6(b) and Fig. 6(c), leads to the formation of aggregates, although there are still parts that look like sheets. This indicates metal impregnation on the material affects the surface morphologies. The percentage composition and content of the elements are presented in Table 3.

Table 3 shows the results of the EDX analysis of the contents and composition of the elements in the catalyst.

**Table 3.** Elements composition of AC, Ni/AC, and Mo/AC catalysts

Element	Content (wt.%)		
	AC	Ni/AC	Mo/AC
Ni	-	6.25	-
Mo	-	-	0.94
C	89.64	87.11	91.13
O	9.60	6.64	7.94
Al	0.50	-	-
K	0.11	-	-
Ca	0.15	-	-

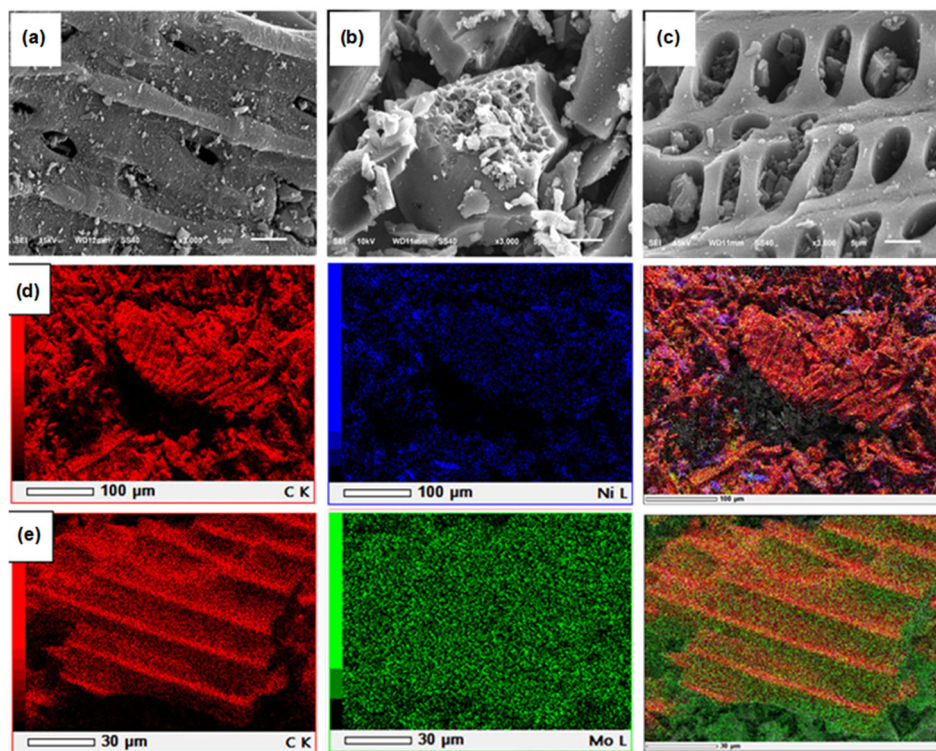


**Fig 6.** SEM images of (a) AC, (b) Ni/AC, and (c) Mo/AC catalysts. SEM mapping of (d) Ni/AC and (e) Mo/AC catalysts

The impregnation of Ni and Mo metals causes a decrease in the content of element C due to the addition of metals in the form of metal oxides. Supportive elements like Al, K, and Ca are gone because of the process of calcination and reduction. The metal in the catalyst does not match its theoretical value of 6%. This may be due to the limitation of SEM analysis, which is only at one point, so the mass calculation of the element on SEM-EDX does not represent the entire sample. The expected Mo content is 6 wt.%, but EDX only found 0.94%. This difference might be because EDX mainly measures the surface and may not detect Mo particles that are located inside pores or below the surface. In contrast, XRD detects crystalline phases throughout the sample, explaining the presence of sharp Mo peaks. Additionally, Mo may not be uniformly distributed, leading to lower localized detection in EDX. The EDX analysis on Ni/AC and Mo/AC catalysts can be observed through mapping results in Fig. 6(d) and 6(e). The Ni and Mo metals were successfully impregnated on the metal surface. The Ni catalysts showed that the distribution of the metal is still uneven and that there are only metal dots on certain parts. On the Mo metal, it has a good spread compared to the Ni metal. The distribution of metal on the forging surface can affect the catalyst's catalytic activity. The evenly scattered metal particles indicate a good spread of the active site.

#### Catalyst Surface Texture Characterization and Acidity Test Using Nitrogen Desorption with Brunauer Emmet Teller and Barrett-Joyner-Teller (BJH) Equation and NH<sub>3</sub>-TPD

The surface area, average porous diameter, and porous volume of AC, Ni/AC, and Mo/AC catalysts are presented in Table 4. According to the size of the pores, activated carbon is distinguished into micropore (< 2 nm), mesopore (2–50 nm), and macropore (> 50 nm) [39]. Based on the results of the analysis, it was obtained that the AC catalyst in the presence of the metal furnace Ni caused the

surface area, volume of pores, and diameter of the pores to increase. The increase in the diameter of the pores occurs because small particles of Ni metal can fill small pores on the surface of AC, leaving large pores. Moreover, the increase in area width and volume of pores is greater when compared to an AC catalyst because the metal Ni does not enter the larger pores, so some of the particles enter the smaller pores and the catalyst surface. In a catalyst, mounted metal Mo decreases the area, volume, and diameter of the pores. The decrease in the catalyst pore's diameter is possible because a large Mo metal fills a large catalytic pore and leaves small pores. The decrease in the surface size and volume of the pores is caused by the presence of agglomerates of Mo metal particles, which decline the surface area and the volume of pores. The decreased volume of pores can also be caused by the presence of metals that stick to the pores' walls and inside them, as seen in Fig. 6(c) and 6(e).

The N<sub>2</sub> isotherm-adsorption curve of the catalyst is classified into 6 types of curves. Classification is divided into type I curves for micropores, curves IV and V for mesopores, and types II, III, and VI for macropores [40]. Based on Fig. 7(a), the curves formed on the AC, Ni/AC, and Mo/AC catalysts are type IV, indicating that the material is mesoporous. This is reinforced by Table 4, where the diameter of the catalytic pores is more than 2 nm. The hysteresis loop on the catalyst belongs to the H4 type that marks mesoporous material.

The pore distribution of the AC, Ni/AC, and Mo/AC catalysts is shown in Fig. 7(b). The diffusion of the catalyst pores is in the range of 2 to 14 nm and is dominated by the size of 2–4 nm. The porous distribution is quite widespread because the metal impregnation is done manually by hand, but the size of the catalytic pores varies greatly at sizes below 4 nm and matches the average size of the pore diameter after impregnation of the metal. Catalyst acidity was tested and

**Table 4.** Surface characteristics of AC, Ni/AC, and Mo/AC catalysts

Catalyst	Surface area (m <sup>2</sup> g <sup>-1</sup> )	Pore volume (cm <sup>3</sup> g <sup>-1</sup> )	Pore diameter (nm)
AC	753.72	0.66	3.52
Ni/AC	803.89	0.77	3.85
Mo/AC	746.68	0.63	3.39

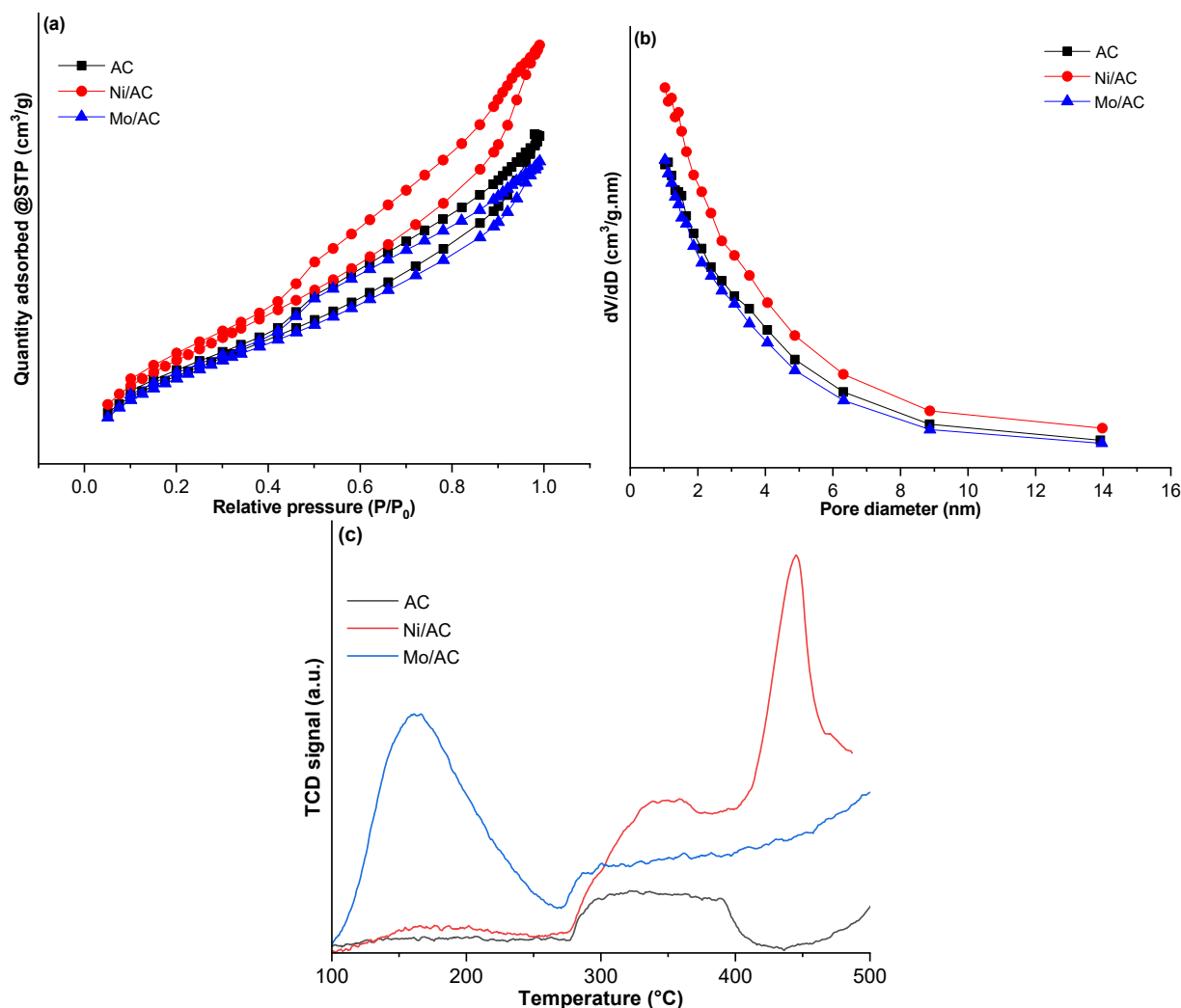


**Fig 7.** (a) Isotherm adsorption-desorption curve, (b) pore distribution curves, (c) NH<sub>3</sub>-TPD analysis curve of AC, Ni/AC, and Mo/AC catalyst

characterized using NH<sub>3</sub>-TPD, as shown in Fig. 7(c). The desorption peak divided into a temperature range of 150–350 °C indicates a weak acid site, while a desorption peak in the temperature range > 350 °C indicates strong acid sites [41]. As shown in Fig. 7(c), the Ni/AC and Mo/AC catalysts have acid site peaks, which indicate metal impregnation affects catalyst acidity.

### Catalytic Activity and Selectivity Test

The result of the catalytic activity of palm cooking oil hydrotreatment into biojet fuel using semi-batch double reactor is shown in Table 5. Table 5 shows that the liquid product conversion of the thermal method, AC, single-layer Ni/AC, single layer Mo/AC, double layer Ni/AC,

double layer Mo/AC, and lower layer Ni/AC with upper layer Mo/AC in the sequence was 27.39, 24.01, 26.21, 24.88, 27.62, 27.05, and 28.43 wt.%. The liquid product conversion result is shown in Fig. 8, which has a clear yellow color similar to the feed. The conversion of liquid products using non-impregnated AC catalysts results in lower conversions and yields than the presence of metals on the catalyst. The presence of acid sites from the metal increases catalytic activity and produces an optimal liquid product. The percentage of liquid product Ni/AC double layer, Mo/AC dual layer, Ni/AC lower layer, and Mo/AC top layer indicate relatively high product conversion compared to a single layer. A double layer on the catalyst can improve stability and enhance contact

**Table 5.** Product distribution and biojet fuel yield from palm oil conversion using different catalysts and methods

Catalyst	Liquid product (wt.%)	Yield (wt.%)				Biojet fuel selectivity (%)
		Biojet fuel	Oxygenates	Non biojet fuel	Main biojet fuel	
Thermal	27.39	19.31	3.74	4.34	9.74	67.45
AC	24.01	20.50	2.18	1.33	8.86	81.89
Ni/AC	26.21	23.69	0.18	2.34	10.57	91.59
Mo/AC	24.88	21.26	2.51	1.01	8.11	85.56
Ni/AC double layer	27.62	24.39	2.66	0.58	8.93	87.93
Mo/AC double layer	27.05	23.94	2.13	0.98	8.14	87.03
Ni/AC-Mo/AC	28.43	24.75	1.99	1.69	10.32	87.21

**Fig 8.** Pictures of feed (Left) and biojet fuel (Right) from palm cooking oil hydrotreatment

performance between catalysts with a higher reactor. Meanwhile, single-layer catalyst conversion results are lower compared with double layer. A single layer may only react with a rapid reactor, so the catalytic performance against the reactor is less than optimal. A single layer has a high particle density that creates a lower contact frequency between the catalyst and the feed.

The use of dual-layer catalysts affects different results. Different types of catalysts, namely Ni/AC and Mo/AC, provide a higher product conversion than dual-layered catalysts Ni/AC and Mo/AC. Differently different types have their respective functions and characteristics. The Ni/AC catalyst works on a hydrocracking reaction to break down long chain molecules to shorter because it has a high hydrogenation activity. Meanwhile, the Mo/AC catalyst has a higher activity on the HDO reaction, eliminating the oxygen content to get more saturated molecules but leaving more oxygenates than the Ni/AC catalyst. Even though Mo/AC

is more effective at HDO reactions, it may not completely convert some functional groups that contain oxygen, leaving behind chemicals that are still oxidized. In contrast, the Ni/AC catalyst has a lower amount of oxidized compounds. This implies that the final product contains significantly fewer oxygenated compounds. This distinction makes it clear that Ni/AC can reduce more things than Mo/AC can, while Mo/AC can only reduce certain HDOs. Combining these two types of catalysts provides a higher activity and selectivity level than a similar catalyst. The compound distribution of double-layer Ni/AC-Mo/AC catalysts during the HDO run is shown in Table 6.

Based on Table 6, yields of biojet fuel in fractions I and II were 20.85 and 3.90 wt.%, respectively. Main biojet fuels yields were 9.03 and 1.28 wt.%. The highest concentration of hydrocarbon compounds in fraction I was 1.98% of pentadecane, and in the fraction II it was 0.35 wt.% of 1-decene. The Ni/AC-Mo/AC catalyst selectivity in fractions I and II was 86.93 and 87.48 wt.%. The double-layer Ni/AC-Mo/AC catalyst is the best performing double-layer catalyst based on the selectivity and yield of the biojet fuel produced. This sequence results in product conversion of 28.43%, selectivity of 87.03%, and biojet fuel yields of 24.75%. This arrangement is better because it uses two different types of catalysts and has their specific functions. The Ni/AC catalyst has specific capabilities in hydrocarbon reactions that dissolve C-C bonds in the carbon chain, whereas Mo/AC can break the C-O bond in the carbon chain for lower oxygen compound content. As for comparison, standard commercial jet fuel composition was shown in Table 7.

**Table 6.** Composition of liquid products from hydrotreating palm cooking oil with double-layer Ni/AC-Mo/AC catalysts based on GC-MS analysis

Retention time (min)	Similarity index	Compound name	Compound formula	Fraction 1 yield (wt.%)	Fraction 2 yield (wt.%)	Total yield (wt.%)
3.66	97	1-Heptene	C <sub>7</sub> H <sub>14</sub>	1.31	0.13	1.44
3.83	97	Heptane	C <sub>7</sub> H <sub>16</sub>	0.95	-	0.95
5.66	95	Toluene	C <sub>7</sub> H <sub>8</sub>	-	0.08	0.08
6.58	96	1-Octene	C <sub>8</sub> H <sub>16</sub>	1.80	0.18	1.98
6.91	97	Octane	C <sub>8</sub> H <sub>18</sub>	1.41	0.05	1.46
7.83	95	Cycloheptene	C <sub>8</sub> H <sub>14</sub>	0.17	-	0.17
9.57	88	Xylene	C <sub>8</sub> H <sub>10</sub>	-	0.04	0.04
10.57	96	1-Nonene	C <sub>9</sub> H <sub>18</sub>	1.64	0.28	1.92
10.93	97	Nonane	C <sub>9</sub> H <sub>20</sub>	1.60	0.11	1.71
12.71	87	4-Nonyne	C <sub>9</sub> H <sub>16</sub>	0.18	0.03	0.21
13.22	94	1-Ethyl-2-methylbenzene	C <sub>9</sub> H <sub>12</sub>	-	0.03	0.03
14.50	95	1-Decene	C <sub>10</sub> H <sub>20</sub>	1.24	0.35	1.59
14.84	97	Decane	C <sub>10</sub> H <sub>22</sub>	0.55	0.14	0.69
15.13	93	2-Decene	C <sub>10</sub> H <sub>20</sub>	0.17	0.04	0.21
18.14	96	1-Undecene	C <sub>11</sub> H <sub>22</sub>	1.04	0.29	1.33
18.44	96	Undecane	C <sub>11</sub> H <sub>24</sub>	0.45	0.12	0.57
18.58	89	2-Undecene	C <sub>11</sub> H <sub>22</sub>	-	0.04	0.04
18.59	95	Cyclopropane	C <sub>11</sub> H <sub>22</sub>	0.49	-	0.49
18.88	95	1-Heptyl-2-methylcyclopropane	C <sub>11</sub> H <sub>22</sub>	0.23	-	0.23
19.28	87	3-Dodecyne	C <sub>12</sub> H <sub>22</sub>	-	0.03	0.03
20.00	73	Naphthalene	C <sub>12</sub> H <sub>14</sub>	-	0.04	0.04
21.47	97	1-Dodecene	C <sub>12</sub> H <sub>24</sub>	0.64	0.22	0.86
21.74	96	Dodecane	C <sub>12</sub> H <sub>26</sub>	0.44	0.12	0.56
24.57	96	1-Tridecene	C <sub>13</sub> H <sub>26</sub>	0.71	0.21	0.92
24.58	96	1-Tridecene	C <sub>13</sub> H <sub>26</sub>	0.89	-	0.89
24.82	97	Tridecane	C <sub>13</sub> H <sub>28</sub>	0.66	0.14	0.80
27.48	97	3-Hexadecene		-	0.24	0.24
27.70	97	Tetradecane	C <sub>14</sub> H <sub>30</sub>	0.47	0.10	0.57
30.19	97	1-Pentadecane	C <sub>15</sub> H <sub>30</sub>	0.60	0.13	0.73
30.42	96	Pentadecane	C <sub>15</sub> H <sub>32</sub>	1.98	-	1.98
30.42	96	Hexadecane	C <sub>16</sub> H <sub>34</sub>	-	0.25	0.25
Biojet fuel yield (C <sub>7</sub> -C <sub>16</sub> )				20.85	3.90	24.75
Main biojet fuel yield [42]				9.03	1.28	10.32
Total selectivity (%)				86.93	87.48	87.21

**Table 7.** Composition of commercial jet fuels using GC-MS

Retention time (min)	Similarity index	Compound name	Compound formula	GC-area (%)
6.892	97	<i>n</i> -Octane	C <sub>8</sub> H <sub>18</sub>	1.06
9.592	95	1,3-Dimethylbenzene	C <sub>8</sub> H <sub>10</sub>	0.92
10.515	94	1,2-Dimethylbenzene	C <sub>8</sub> H <sub>10</sub>	1.04
10.892	97	<i>n</i> -Nonane	C <sub>9</sub> H <sub>20</sub>	2.29

Retention time (min)	Similarity index	Compound name	Compound formula	GC-area (%)
12.100	95	Propylcyclohexane	C <sub>9</sub> H <sub>18</sub>	0.77
12.242	95	3-Methylnonane	C <sub>10</sub> H <sub>22</sub>	0.89
12.969	96	Propylbenzene	C <sub>9</sub> H <sub>12</sub>	0.66
13.276	93	1-Ethyl-3-methylbenzene	C <sub>9</sub> H <sub>12</sub>	1.75
13.472	90	2-Methylnonane	C <sub>10</sub> H <sub>22</sub>	1.01
13.714	92	2,6-Dimethyloctane	C <sub>10</sub> H <sub>22</sub>	1.07
14.208	95	1-Methyl-2-propylcyclohexane	C <sub>10</sub> H <sub>20</sub>	1.14
14.561	88	1,2,3-Trimethylbenzene	C <sub>9</sub> H <sub>12</sub>	1.62
14.873	97	<i>n</i> -Decane	C <sub>10</sub> H <sub>22</sub>	5.25
15.147	96	1-Methylpropylbenzene	C <sub>10</sub> H <sub>14</sub>	1.23
15.654	96	2,5,5-Trimethylheptane	C <sub>10</sub> H <sub>22</sub>	3.79
16.042	94	Butylcyclohexane	C <sub>10</sub> H <sub>20</sub>	1.43
16.239	95	3,7-Dimethylnonane	C <sub>11</sub> H <sub>24</sub>	0.69
16.546	97	1,2-Diethylbenzene	C <sub>10</sub> H <sub>14</sub>	0.76
16.677	88	1-Methyl-2-propylbenzene	C <sub>10</sub> H <sub>14</sub>	1.02
16.904	89	1,2,4,5-Tetrametilbenzene	C <sub>10</sub> H <sub>14</sub>	1.60
17.032	95	4-Methyldecane	C <sub>11</sub> H <sub>24</sub>	1.26
17.199	94	2-Methyldecane	C <sub>11</sub> H <sub>24</sub>	1.73
17.414	92	3-Methyldecane	C <sub>11</sub> H <sub>24</sub>	1.14
17.664	95	1-Methyl-3-isopropylbenzene	C <sub>10</sub> H <sub>14</sub>	1.65
17.896	96	4-Ethyl- <i>o</i> -xylene	C <sub>10</sub> H <sub>14</sub>	1.16
18.058	91	Bicyclo[3,1,1]heptane	C <sub>13</sub> H <sub>22</sub>	1.13
18.504	97	Dodecane	C <sub>12</sub> H <sub>26</sub>	8.12
19.004	95	1-Dodecyne	C <sub>12</sub> H <sub>22</sub>	1.95
19.125	87	1,2,4,5-Tetramethylbenzene	C <sub>10</sub> H <sub>14</sub>	0.95
19.338	93	Tridecane	C <sub>13</sub> H <sub>28</sub>	0.86
19.532	96	Decahydro-2-methylnaphthalene	C <sub>11</sub> H <sub>20</sub>	0.82
19.683	96	Hexylcyclohexane	C <sub>12</sub> H <sub>24</sub>	0.95
19.794	97	1-Dodecene	C <sub>12</sub> H <sub>24</sub>	1.31
20.244	94	2,5-Dimethyldecane	C <sub>12</sub> H <sub>26</sub>	2.45
20.436	95	4-Methylundecane	C <sub>12</sub> H <sub>26</sub>	1.13
20.558	90	2-Ethyltetralin	C <sub>12</sub> H <sub>16</sub>	2.43
20.811	92	Tridecane	C <sub>13</sub> H <sub>28</sub>	0.94
21.190	95	2,3-Dimethylundecane	C <sub>13</sub> H <sub>28</sub>	1.24
21.360	93	Naphthalene	C <sub>10</sub> H <sub>8</sub>	1.78
21.820	93	Tridecane	C <sub>13</sub> H <sub>28</sub>	7.59
22.180	91	2,6-Dimethylundecane	C <sub>13</sub> H <sub>28</sub>	1.98
22.339	86	1,2,3,4-Tetrahydro-2-methyl naphthalene	C <sub>11</sub> H <sub>14</sub>	1.12
22.505	85	<i>trans-syn</i> -Tricyclo 7,3,0,0(2,6)-8-dodecane 7,3,0,0(2,6)	C <sub>12</sub> H <sub>18</sub>	1.25
23.069	97	1-Cyclohexane	C <sub>12</sub> H <sub>24</sub>	1.42
23.376	91	6-Methyldodecane	C <sub>13</sub> H <sub>28</sub>	1.33
23.592	93	4-Methyldodecane	C <sub>13</sub> H <sub>28</sub>	0.66
23.763		2-Methyldodecane	C <sub>13</sub> H <sub>28</sub>	1.44
24.002	94	4,6-Dimethyldodecane	C <sub>14</sub> H <sub>30</sub>	2.84
24.180	94	1,1,3-Trimethyl-2-(3-methylpentyl)cyclohexane	C <sub>15</sub> H <sub>30</sub>	0.68

Retention time (min)	Similarity index	Compound name	Compound formula	GC-area (%)
24.643	88	1,2,3,4-Tetrahydro-5-methylnaphthalene	C <sub>11</sub> H <sub>14</sub>	1.42
24.889	87	Tridecane	C <sub>13</sub> H <sub>28</sub>	5.56
25.162	92	3,4-Trimethyldecene	C <sub>12</sub> H <sub>24</sub>	0.87
25.324	94	2-Methyldodecane	C <sub>13</sub> H <sub>28</sub>	0.79
25.550	93	1,2,3,4-Tetrahydro-2,7-dimethylnaphthalene	C <sub>12</sub> H <sub>16</sub>	0.92
26.211	94	Octyl-cyclohexane	C <sub>14</sub> H <sub>28</sub>	1.54
26.700	95	Tetradecane	C <sub>14</sub> H <sub>30</sub>	0.82
27.025	94	2,7,10-Trimethyldodecane	C <sub>15</sub> H <sub>32</sub>	1.22
27.700	97	Heptadecane	C <sub>17</sub> H <sub>36</sub>	2.77
30.417	97	Heptadecane	C <sub>17</sub> H <sub>36</sub>	0.76

**Table 8.** Comparison of biojet fuel selectivity with other studies

Catalyst	Feed	Reactor type	Condition	Biojet fuel selectivity (%)	Reference
Ni/AC-Mo/AC	Palm cooking oil	Semi-batch double	400–550 °C, 20 mL/min of H <sub>2</sub> gas flow	87.21	Present work
Ni/NH <sub>4</sub> -Beta	Palm olein	Batch	360 °C, 39.47 atm	36.60	[43]
R5-TaPa	Date palm seed oil	Batch	400 °C, 9.86 atm of H <sub>2</sub>	53.60	[44]
CoW/SA	Tung oil	Semi-batch	350–400 °C, 20 mL/min of N <sub>2</sub> gas flow	60.00	[45]
Co/ZnO	Safflower oil	Batch	350 °C, 74 atm	65.96	[46]

Commercial jet fuels have hydrocarbons in the C<sub>8</sub>–C<sub>16</sub> carbon atom range that is dominated by the C<sub>10</sub>–C<sub>12</sub> carbon chain. Liquid products obtained from the hydrotreating of palm cooking oil into biojet fuel using AC, Ni/AC, Ni/AC-Ni/AC, Mo/AC, Mo/AC-Mo/AC and Ni/AC-Mo/AC catalysts are still in the range of commercial jet fuel hydrocarbons. According to Benavides et al. [42], the main biojet fuel yield (jet fuel A and jet fuel A-1) are hydrocarbons that have a C<sub>7</sub>–C<sub>16</sub> carbon range, including alkanes, alkenes, cycloalkenes, alkynes, and aromatic compounds. The use of catalysts in hydrotreating palm cooking oil has successfully improved the biojet fuel selectivity. There is no reusability test after determining the best-performing catalyst because this research was aimed to study the effect of catalyst arrangement on catalytic activity and selectivity. Table 8 shows the catalytic selectivity of different studies and methods on biojet fuel conversion. The Ni/AC-Mo/AC catalyst has the highest bio-jet fuel selectivity. Compared to others, the present work only used 1 atm of pressure via H<sub>2</sub> gas flow, which is a much lower pressure required than those carried out by Chintakanan et al. [43], Rambabu et

al. [44], and Çakan et al. [46] resulting in less energy needed for the hydrotreating reaction.

## ■ CONCLUSION

Based on the research that has been done, it can be concluded that the catalysts AC, Ni/AC, and Mo/AC were successfully synthesized by the sprayed dry impregnation method. The resulting catalyst has a successive surface area of 753.72, 803.90, and 746.68 m<sup>2</sup> g<sup>-1</sup>, consecutive pore volume of 0.66, 0.77, and 0.63 cm<sup>3</sup> g<sup>-1</sup>, and consecutive porous diameter of 3.52, 3.85, and 3.39 nm. The Ni and Mo metal content of the Ni/AC and Mo/AC catalysts is 6.25 and 0.94%, respectively. The catalyst sequence in a double-batch reactor produces the optimum activity, selectivity, and yield of biojet fuel found in the Ni/AC-Mo/AC catalysts sequence. Layers of a catalyst affect the catalytic performance in activity and selectivity where Ni/AC-Mo/AC catalyst produces 28.42 wt.% liquid hydrocarbon product, 86.93 (fraction I) and 87.48% (fraction II) selectivity, and biojet fuel yield of 24.75 wt.%. Therefore, catalyst layer arrangement affects

the catalytic activity and selectivity in palm cooking oil hydrotreatment into biojet fuel.

## ■ ACKNOWLEDGMENTS

The authors gratefully thank Universitas Gadjah Mada for financially supporting the research under the RTA 2024 project (Contract number: 4971/UN1.P1/PT.01.01/2024).

## ■ CONFLICT OF INTEREST

The authors declared to have no conflict of interest.

## ■ AUTHOR CONTRIBUTIONS

Wega Trisunaryanti: conceptualization, supervision, validation, methodology, writing, review and editing; Karna Wijaya: data curation; Muhammad Darul Ikhsan Saputro: formal analysis, writing original draft. All authors have read and agreed to the final version of this manuscript.

## ■ REFERENCES

- [1] Barke, A., Bley, T., Thies, C., Weckenborg, C., and Spengler, T.S., 2022, Are sustainable aviation fuels a viable option for decarbonizing air transport in Europe? An environmental and economic sustainability assessment, *Appl. Sci.*, 12 (2), 597.
- [2] Planès, T., Delbecq, S., Pommier-Budinger, V., and Bénard, E., 2021, Simulation and evaluation of sustainable climate trajectories for aviation, *J. Environ. Manage.*, 295, 113079.
- [3] Fitriasari, E.I., Won, W., and Jay Liu, J., 2023, Sustainability assessment of biojet fuel produced from pyrolysis oil of woody biomass, *Sustainable Energy Fuels*, 7 (15), 3625–2626.
- [4] Ishaq, M., Ghouse, G., Fernández-González, R., Puime-Guillén, F., Tandir, N., and Santos de Oliveira, H.M., 2022, From fossil energy to renewable energy: Why is circular economy needed in the energy transition?, *Front. Environ. Sci.*, 10, 941791.
- [5] Abdullah, A.A., 2021, Global effects of atmospheric emissions, *NeuroQuantology*, 19 (5), 25–34.
- [6] Alikishiyev, A., and Dusserre, G., 2022, Carbon-dioxide emissions due to fossil fuels consumption, *J. Energy Resour. Convers.*, 2 (1), 1–16.
- [7] Björnsson, L., and Ericsson, K., 2024, Emerging technologies for the production of biojet fuels from wood—can greenhouse gas emission reductions meet policy requirements?, *Biomass Convers. Biorefin.*, 14 (6), 7603–7622.
- [8] Carli, M.F., Susanto, B.H., and Habibie, T.K., 2018, Synthesis of bioavtural through hydrodeoxygenation and catalytic cracking from oleic acid using NiMo/zeolite catalyst, *E3S Web Conf.*, 67, 02023.
- [9] Eller, Z., Varga, Z., and Hancsók, J., 2016, Advanced production process of jet fuel components from technical grade coconut oil with special hydrocracking, *Fuel*, 182, 713–720.
- [10] Siregar, M.A., Sembiring, S.A., and Ramli, R., 2014, The price of palm-cooking oil in Indonesia: Antecedents and consequences on the international price and the export volume of CPO, *J. Econ. Sustainable Dev.*, 5 (23), 227–235.
- [11] Hidayat, A., Robiani, B., Marwa, T., and Suhel, S., 2023, Competitiveness, market structure, and energy policies: A case study of the world's largest crude palm oil exporter, *Int. J. Energy Econ. Policy*, 13 (3), 111–121.
- [12] Nurulain, S., Aziz, N.A., Najib, M.S., Salim, M.R., and Manap, H., 2021, A review of free fatty acid determination methods for palm cooking oil, *J. Phys.: Conf. Ser.*, 1921 (1), 012055.
- [13] Itthibenchapong, V., Srifa, A., Kaewmeesri, R., Kidkhunthod, P., and Faungnawakij, K., 2017, Deoxygenation of palm kernel oil to jet fuel-like hydrocarbons using Ni-MoS<sub>2</sub>/γ-Al<sub>2</sub>O<sub>3</sub> catalysts, *Energy Convers. Manage.*, 134, 188–196.
- [14] Tsiotsias, A.I., Hafeez, S., Charisiou, N.D., Al-Salem, S.M., Manos, G., Constantinou, A., AlKhoori, S., Sebastian, V., Hinder, S.J., Baker, M.A., Polychronopoulou, K., and Goula, M.A., 2023, Selective catalytic deoxygenation of palm oil to produce green diesel over Ni catalysts supported on ZrO<sub>2</sub> and CeO<sub>2</sub>-ZrO<sub>2</sub>: Experimental and process simulation modelling studies, *Renewable Energy*, 206, 582–596.
- [15] Murachman, B., Deendarlianto, D., Nissaraly, H.F.,

- and Hasyim, W., 2014, Experimental study on hydrocracking process of asbuton hydrocarbon based on the aromatic, and waxy residue based on paraffinic, by using Pt/Pd and  $\gamma$ -alumina catalyst in a fixed bed reactor, *ASEAN J. Chem. Eng.*, 14 (1), 59–75.
- [16] Corma, A., and Orchillés, A.V., 2000, Current views on the mechanism of catalytic cracking, *Microporous Mesoporous Mater.*, 35-36, 21–30.
- [17] Yani, F.T., Husin, H., Darmadi, D., Muhammad, S., Abnisa, F., Nurhazanah, N., Nasution, F., and Erdiwansyah, E., 2022, Palm oil hydrodeoxygenation into green diesel over NiO/NbOPO<sub>4</sub> catalyst: A novel approach of synthesizing NbOPO<sub>4</sub> from NbCl<sub>5</sub>, *J. Cleaner Prod.*, 354, 131704.
- [18] Yang, C., Wang, W., Wang, D., Gong, M., Xin, Y., Xiao, L., Kikhtyanin, O.V., Kubicka, D., and Wu, W., 2022, The promotion effects of MoO<sub>x</sub> species in the highly effective NiMo/MgAl<sub>2</sub>O<sub>4</sub> catalysts for the hydrodeoxygenation of methyl palmitate, *J. Environ. Chem. Eng.*, 10 (3), 107761.
- [19] Trisunaryanti, W., Triyono, T., Purwono, S., Purwanti, A.S., and Sumbogo, S.D., 2022, Synthesis of mesoporous carbon from merbau sawdust as a nickel metal catalyst support for castor oil hydrocracking, *Bull. Chem. React. Eng. Catal.*, 17 (1), 216–224.
- [20] Ma, B., and Zhao, C., 2015, High-grade diesel production by hydrodeoxygenation of palm oil over a hierarchically structured Ni/HBEA catalyst, *Green Chem.*, 17 (3), 1692–1701.
- [21] Sasaki, T., Kasai, H., and Nishibori, E., 2019, Aspherical and covalent bonding character of d electrons of molybdenum from synchrotron X-ray diffraction, *J. Phys. Commun.*, 3 (9), 095009.
- [22] Visiamah, F., Trisunaryanti, W., and Triyono, T., 2024, Microwave-assisted coconut wood carbon-based catalyst impregnated by Ni and/or Pt for bio-jet fuel range hydrocarbons production from *Calophyllum inophyllum* L. oil using modified-microwave reactor, *Case Stud. Chem. Environ. Eng.*, 9, 100722.
- [23] Dahdah, E., Estephane, J., Gennequin, C., Aboukais, A., Abi-Aad, E., and Aouad, S., 2020, Zirconia supported nickel catalysts for glycerol steam reforming: Effect of zirconia structure on the catalytic performance, *Int. J. Hydrogen Energy*, 45 (7), 4457–4467.
- [24] Trisunaryanti, W., Wijaya, K., Kartini, I., Purwono, S., Rodiansono, R., Mara, A., and Rahma, A.S., 2024, Hydrodeoxygenation of refined palm kernel oil (RPKO) into bio-jet fuel using Mo/H-ZSM-5 catalysts, *React. Kinet., Mech. Catal.*, 137 (2), 843–878.
- [25] Campbell, C.T., Parker, S.C., and Starr, D.E., 2002, The effect of size-dependent nanoparticle energetics on catalyst sintering, *Science*, 298 (5594), 811–814.
- [26] Wijaya, K., Kurniawan, M.A., Saputri, W.D., Trisunaryanti, W., Mirzan, M., Hariani, P.L., and Tikoalu, A.D., 2021, Synthesis of nickel catalyst supported on ZrO<sub>2</sub>/SO<sub>4</sub> pillared bentonite and its application for conversion of coconut oil into gasoline via hydrocracking process, *J. Environ. Chem. Eng.*, 9 (4), 105399.
- [27] Zięzio, M., Charnas, B., Jedynak, K., Hawryluk, M., and Kucio, K., 2020, Preparation and characterization of activated carbons obtained from the waste materials impregnated with phosphoric acid(V), *Appl. Nanosci.*, 10 (12), 4703–4716.
- [28] Trisunaryanti, W., Wijaya, K., Triyono, T., Wahyuningtyas, N., Utami, S.P., and Larasati, S., 2022, Characteristics of coconut shell-based activated carbon as Ni and Pt catalyst supports for hydrotreating *Calophyllum inophyllum* oil into hydrocarbon-based biofuel, *J. Environ. Chem. Eng.*, 10 (5), 108209.
- [29] Klasson, K.T., Ledbetter, C.A., Uchimiya, M., and Lima, I.M., 2013, Activated biochar removes 100 % dibromochloropropane from field well water, *Environ. Chem. Lett.*, 11 (3), 271–275.
- [30] Munnik, P., de Jongh, P.E., and de Jong, K.P., 2015, Recent developments in the synthesis of supported catalysts, *Chem. Rev.*, 115 (14), 6687–6718.
- [31] Triyono, T., Trisunaryanti, W., Purbonegoro, J., and Aksanti, S.I., 2024, Effect of cobalt impregnation methods on Parangtritis sand towards catalysts activity in hydrocracking of

- degummed low-quality Ujung Kulon Malapari oil into biohydrocarbons, *React. Kinet., Mech. Catal.*, 137 (1), 303–321.
- [32] Park, S.B., Park, J.E., Na, G., Choi, C., Cho, Y.H., and Sung, Y.E., 2023, Low-cost and high-performance anion-exchange membrane water electrolysis stack using non-noble metal-based materials, *ACS Appl. Energy Mater.*, 6 (17), 8738–8748.
- [33] Abioye, A.M., Noorden, Z.A., and Ani, F.N., 2017, Synthesis and characterizations of electroless oil palm shell based-activated carbon/nickel oxide nanocomposite electrodes for supercapacitor applications, *Electrochim. Acta*, 225, 493–502.
- [34] Bakti, A.I., and Gareso, P.L., 2018, Characterization of active carbon prepared from coconuts shells using FTIR, XRD and SEM techniques, *JIPF Al-Biruni*, 7 (1), 33–39.
- [35] Taer, E., Nikmatun, N., Apriwandi, A., Agustino, A., Taslim, R., and Hidayat, E., 2021, The self-adhesive carbon powder based on coconut coir fiber as supercapacitor application, *J. Metastable Nanocryst. Mater.*, 33, 1–11.
- [36] Riahi, K.Z., Sdiri, N., Ennigrou, D.J., and Horchani-Naifer, K., 2020, Investigations on electrical conductivity and dielectric properties of graphene oxide nanosheets synthesized from modified Hummer's method, *J. Mol. Struct.*, 1216, 128304.
- [37] Wijaya, K., Nadia, A., Dinana, A., Pratiwi, A.F., Tikoalu, A.D., and Wibowo, A.C., 2021, Catalytic hydrocracking of fresh and waste frying oil over Ni- and Mo-based catalysts supported on sulfated silica for biogasoline production, *Catalysts*, 11 (10), 1150.
- [38] Huang, J., Xu, Z., Cao, L., Zhang, Q., Ouyang, H., and Li, J., 2015, Tailoring MoO<sub>2</sub>/graphene oxide nanostructures for stable, high-density sodium-ion battery anodes, *Energy Technol.*, 3 (11), 1108–1114.
- [39] Rasyid, R., Wicaksono, R.A.S., Lusita, D.D., Mahfud, M., and Roesyadi, A., 2015, Efektifitas katalis Co/Mo pada hydrocracking minyak nyamplung, *Reaktor*, 15 (4), 268–273.
- [40] Thommes, M., Kaneko, K., Neimark, A.V., Olivier, J.P., Rodriguez-Reinoso, F., Rouquerol, J., and Sing, K.S.W., 2015, Physisorption of gases, with special reference to the evaluation of surface area and pore size distribution (IUPAC Technical Report), *Pure Appl. Chem.*, 87 (9-10), 1051–1069.
- [41] Mosallanejad, S., Dlugogorski, B.Z., Kennedy, E.M., and Stockenhuber, M., 2018, On the chemistry of iron oxide supported on  $\gamma$ -alumina and silica catalysts, *ACS Omega*, 3 (5), 5362–5374.
- [42] Benavides, A., Benjumea, P., Cortés, F.B., and Ruiz, M.A., 2021, Chemical composition and low-temperature fluidity properties of jet fuels, *Processes*, 9 (7), 1184.
- [43] Chintakanan, P., Vitidsant, T., Reubroycharoen, P., Kuchonthara, P., Kida, T., and Hinchiranan, N., 2021, Bio-jet fuel range in biofuels derived from hydroconversion of palm olein over Ni/zeolite catalysts and freezing point of biofuels/Jet A-1 blends, *Fuel*, 293, 120472.
- [44] Rambabu, K., Bharath, G., Sivarajasekar, N., Velu, S., Sudha, P.N., Wongsakulphasatch, S., and Banat, F., 2023, Sustainable production of bio-jet fuel and green gasoline from date palm seed oil via hydroprocessing over tantalum phosphate, *Fuel*, 331, 125688.
- [45] Asikin-Mijan, N., AbdulKareem-Alsultan, G., Mastuli, M.S., Salmiaton, A., Azuwa Mohamed, M., Lee, H.V., and Taufiq-Yap, Y.H., 2022, Single-step catalytic deoxygenation-cracking of tung oil to bio-jet fuel over CoW/silica-alumina catalysts, *Fuel*, 325, 124917.
- [46] Çakan, A., Kiren, B., and Ayas, N., 2023, Hydrodeoxygenation of safflower oil over cobalt-doped metal oxide catalysts for bio-aviation fuel production, *Mol. Catal.*, 546, 113219.